Japanese Journal of Applied Physics

The Japan Society of Applied Physics

REGULAR PAPER

Quantification of limitations in statistical analysis of ultrasound echo envelope amplitudes

To cite this article: Shohei Mori *et al* 2023 *Jpn. J. Appl. Phys.* **62** SJ1045

View the article online for updates and enhancements.

You may also like

- Imaging the elastic properties of tissue: the 20 year perspective
K J Parker, M M Doyley and D J Rubens
- Performance criteria for quantitative ultrasonology and image parameterisation
C R Hill, J C Bamber and D O Cosgrove
- Power laws prevail in medical ultrasound
K J Parker

This content was downloaded from IP address 130.34.32.223 on 12/04/2023 at 04:43

Japanese Journal of Applied Physics **62**, SJ1045 (2023) **REGULAR PAPER**
https://doi.org/10.35848/1347-4065/acc33e

Quantification of limitations in statistical analysis of ultrasound echo envelope amplitudes

Shohei Mori[1*], Mototaka Arakawa[1,2], Hiroshi Kanai[1,2], and Hiroyuki Hachiya[3]

[1]Graduate School of Engineering, Tohoku University, Sendai, Miyagi 980-8579, Japan
[2]Graduate School of Biomedical Engineering, Tohoku University, Sendai, Miyagi 980-8579, Japan
[3]School of Engineering, Tokyo Institute of Technology, Meguro, Tokyo 152-8550, Japan

*E-mail: mori@tohoku.ac.jp

Received November 16, 2022; revised February 26, 2023; accepted March 10, 2023; published online April 12, 2023

Ultrasound echo envelope statistics have been widely studied for quantitative tissue characterization. In ultrasound measurements, the size of the region-of-interest (ROI) is limited by several factors, such as the locality of the tissue characteristics and the depth dependence of the acoustic field of the ultrasound beam. In this case, the evaluated echo envelope statistics vary even when the envelope amplitudes follow the same population without any noise. In this study, the statistical variance of the moments caused by this finite number of samples was quantified based on the central limit theorem and the law of error propagation. The proposed principles were validated by random number simulation and used to quantify the statistical variance of Nakagami parameter estimation. Finally, the effective number of independent samples in an ultrasonic measurement was quantified based on the relationship between the ROI size and the ultrasound spatial resolution. © 2023 The Japan Society of Applied Physics

1. Introduction

Medical ultrasound is widely used for the diagnosis of various diseases owing to its noninvasiveness and real-time performance. Ultrasound RF echo signals obtained from biological tissues reflect information on scatterer distribution in the tissue. This scatterer distribution changes according to tissue characteristics; therefore, an estimation of the scatterer distribution characteristics from ultrasound RF echo signals contributes to the diagnosis of various diseases.

Echo envelope statistics have been widely studied to evaluate the characteristics of scatterer distribution.[1,2] In the most common approaches for statistics-based tissue characterization, the probability density function of the echo envelope amplitudes is fitted by a model function, and the scatterer distribution characteristics are quantified by model parameters. Various model functions have been used to quantify scatterer distribution characteristics, such as Rayleigh,[3–5] Nakagami,[6–8] K,[9,10] homodyned-K,[11–14] multi-Rayleigh,[15–18] and double-Nakagami[19–22] models. Based on these model functions, various tissue characterization methods have been proposed, such as quantitative tissue characterization methods for the liver,[15–24] skin,[25,26] and lymph nodes,[27,28] and evaluation methods for temperature changes in biological tissues.[29–31]

In these model functions, the model parameters are related to the scatterer distribution characteristics. Therefore, the tissue characteristics can be quantified using the model parameters. In general, the relationship between model parameters and scatterer distribution characteristics is theoretically quantified under the condition that infinite-length data can be obtained.

However, in actual ultrasonic measurements, the number of samples, i.e. the size of the region of interest (ROI), is limited owing to several factors, such as the locality of the tissue characteristics and the depth dependence of the acoustic field of the ultrasound beam. Under the condition of a limited number of samples, the statistical properties of the obtained data vary, as indicated by the central limit theorem. This variation is caused even under conditions in which there is no noise, the depth dependence of the acoustic field can be completely compensated, and the obtained echo envelope signals follow the exact same population. This is a limitation in the statistical analysis of echo envelope amplitudes; therefore, it is essential to understand this limitation for accurate tissue characterization.

In this study, we theoretically quantify this statistical limitation based on the central limit theorem and the law of error propagation and evaluate the relationship between the ultrasonic analysis conditions and statistical limitations. In this study, we focus on moments, which are basic statistical properties such as the average, variance, skewness, and kurtosis. Moments have also been used for parameter estimation for model functions[6,9–11,32–34]; therefore, a quantification of the statistical limitations in moment analysis is important.

In our previous study, we examined the statistical variance of non-normalized moments.[35] However, in our previous studies,[17,18,32–34] the signals were normalized by the root of their power because the power depends on the ultrasonic transmitted/received conditions, which complicates the evaluation of the scatterer distribution characteristics. Thus, in this study, we quantify the statistical variance for normalized moments as well as for non-normalized moments. Furthermore, we quantify the statistical covariance between different orders of moments because they are obtained from the same samples and are correlated with each other. Then, we quantify the statistical variance of the Nakagami parameter estimated by the moment method to demonstrate the use of the proposed principles in an analysis of the statistical limitations of tissue characterization. Finally, we conducted an ultrasonic simulation to quantify the effective number of independent samples within the ROI.

2. Principles

2.1. Statistical moment

Statistical moment is a basic statistical property. When independent random variables $\{x_q\}$ with infinite length follow the probability density function $q(x)$, the kth order of the

 © 2023 The Japan Society of Applied Physics

non-normalized moment around the origin, $M_{\mathrm{T}}(k;\, q)$, is defined as

$$M_{\mathrm{T}}(k;\, q) = \mathrm{E}[x_q^k] = \int_{-\infty}^{\infty} x^k q(x)dx, \tag{1}$$

where E[·] denotes the expectation. As shown by Eq. (1), the first order of moment $M_{\mathrm{T}}(1;\, q)$ is the expectation of variables $\{x_q\}$ following $q(x)$. The second, third, and fourth orders of moments are related to information on the power, skewness, and kurtosis of the variables $\{x_q\}$ following $q(x)$, respectively.

2.2. Quantification of statistical variance and covariance of non-normalized moments

Under ultrasonic measurement conditions, the number of samples in the ROI is finite. In this case, the statistical properties of the random variables, such as the statistical moment, vary around the theoretical value even if the random variables follow the exact same population and are independent of each other.

Figure 1 shows examples of random number simulations in which random numbers following the Rayleigh distribution [Fig. 1(a)] were generated and the first and third orders of the non-normalized moments of the random numbers were calculated. The results of the 100 trials are plotted in Figs. 1(b) and 1(c). Figures 1(b) and 1(c) show the moments calculated using 500 and 2000 independent random numbers, respectively. As shown in Fig. 1, the moments obtained from a finite number of samples vary around the theoretical values (red), and this variation can be suppressed by increasing the number of independent samples. This statistical variance caused by the finite number of samples is quantified as follows:

Let $\{x_{q,l}\}_{l=1,2,\cdots,L}$ be L independent random numbers that follow the model function $q(x)$. In ultrasonic measurements, these random numbers are related to echo envelope amplitudes. The finite number of independent samples, L, is determined by the relationship between the area of the ROI and the area of the point spread function (PSF) (i.e. ultrasound spatial resolution),[5] as discussed in the Methods and Results sections. The kth order of the non-normalized moment $M_L(k;\, q)$ for $\{x_{q,l}\}_{l=1,2,\cdots,L}$ is defined as follows:

$$M_L(k;\, q) = \frac{1}{L}\sum_{l=1}^{L} x_{q,l}^k. \tag{2}$$

Let us describe $y_{q_k,l}$ as follows:

$$y_{q_k,l} = x_{q,l}^k. \tag{3}$$

As the sets of $\{x_{q,l}\}$ follow a certain model function $q(x)$, the sets of $\{y_{q_k,l}\}$ also follow a certain model function $q_k(y)$, where $q_k(y)$ differs from $q(y)$. Subsequently, $M_L(k;\, q)$ in Eq. (2) can be expressed as

$$M_L(k;\, q) = \frac{1}{L}\sum_{l=1}^{L} y_{q_k,l}, \tag{4}$$

which shows that the kth order of the moment $M_L(k;\, q)$ for $\{x_{q,l}\}_{l=1,2,\cdots,L}$ is obtained by the average of $\{y_{q_k,l}\}_{l=1,2,\cdots,L}$ following a certain model function $q_k(y)$. As a result of the central limit theorem, the moment $M_L(k;\, q)$ obtained from L independent random numbers follows a normal distribution $N(\mu_{q_k},\, \sigma_{q_k}^2/L)$.

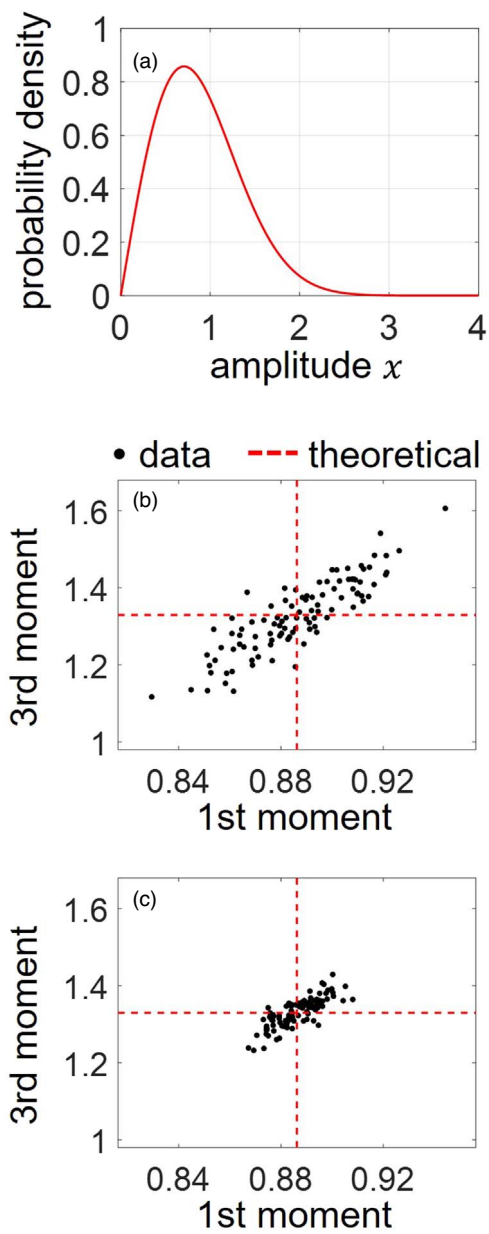

Fig. 1. (a) Probability density function of Rayleigh distribution. (b), (c) First and third orders of non-normalized moments obtained from (b) 500 and (c) 2000 independent random numbers generated from Rayleigh distribution. Results of 100 trials are plotted in (b) and (c).

$$M_L(k;\, q) \in N\left(\mu_{q_k},\, \frac{\sigma_{q_k}^2}{L}\right), \tag{5}$$

where μ_{q_k} and $\sigma_{q_k}^2$ are the expectation and variance of the independent random variables $\{y_{q_k} = x_q^k\}$ with an infinite length following $q_k(y)$, respectively. Here, μ_{q_k} and $\sigma_{q_k}^2$ are given by

$$\mu_{q_k} = \mathrm{E}[y_{q_k}] = \mathrm{E}[x_q^k] = M_{\mathrm{T}}(k;\, q), \tag{6}$$

$$\begin{aligned}\sigma_{q_k}^2 &= \mathrm{E}[(y_{q_k} - \mu_{q_k})^2] = \mathrm{E}[(x_q^k - \mathrm{E}[x_q^k])^2] \\ &= M_{\mathrm{T}}(2k;\, q) - M_{\mathrm{T}}(k;\, q)^2.\end{aligned} \tag{7}$$

Thus, the statistical variance $\sigma_{\mathrm{M}}^2(L,\, k;\, q)$ of the kth order of the non-normalized moment $M_L(k;\, q)$ is determined from the number of independent samples, L, and the theoretical kth

© 2023 The Japan Society of Applied Physics

and $(2k)$th orders of non-normalized moments.

$$\sigma_{\mathrm{M}}^2(L,\,k;\,q) = \frac{M_{\mathrm{T}}(2k;\,q) - M_{\mathrm{T}}(k;\,q)^2}{L}. \tag{8}$$

Because each order of moments is obtained from the same samples, different orders of moments are correlated with each other. This correlation is also an important factor in evaluating the statistical properties of the echo envelope amplitudes. For example, the covariance matrix for several orders of moments can be used to estimate the number of tissue components in a fibrotic liver.[18)]

The statistical covariance between the k_1th and k_2th orders of non-normalized moments can be formulated as follows: First, let us define the summation of the k_1th and k_2th orders of moments as

$$SUM_{\mathrm{T}}(k_1,\,k_2;\,q) = M_{\mathrm{T}}(k_1;\,q) + M_{\mathrm{T}}(k_2;\,q), \tag{9}$$

$$SUM_L(k_1,\,k_2;\,q) = M_L(k_1;\,q) + M_L(k_2;\,q). \tag{10}$$

Then, from the law of error propagation, the following relationship holds:

$$\begin{aligned}\sigma_{\mathrm{SUM}}^2(L,\,k_1,\,k_2;\,q) &= \left(\frac{\partial \mathrm{SUM}_{\mathrm{T}}(k_1,k_2;q)}{\partial M_{\mathrm{T}}(k_1;q)}\right)^2 \sigma_{\mathrm{M}}^2(L,\,k_1;\,q) \\ &\quad + \left(\frac{\partial \mathrm{SUM}_{\mathrm{T}}(k_1,k_2;q)}{\partial M_{\mathrm{T}}(k_2;q)}\right)^2 \sigma_{\mathrm{M}}^2(L,\,k_2;\,q) \\ &\quad + 2\frac{\partial \mathrm{SUM}_{\mathrm{T}}(k_1,k_2;q)}{\partial M_{\mathrm{T}}(k_1;q)}\frac{\partial \mathrm{SUM}_{\mathrm{T}}(k_1,k_2;q)}{\partial M_{\mathrm{T}}(k_2;q)}\mathrm{COV}_{\mathrm{M}}(L,\,k_1,\,k_2;\,q) \\ &= \sigma_{\mathrm{M}}^2(L,\,k_1;\,q) + \sigma_{\mathrm{M}}^2(L,\,k_2;\,q) + 2\mathrm{COV}_{\mathrm{M}}(L,\,k_1,\,k_2;\,q),\end{aligned} \tag{11}$$

where $\sigma_{\mathrm{SUM}}^2(L,\,k_1,\,k_2;\,q)$ is the statistical variance of $SUM_L(k_1,\,k_2;\,q)$ and $\mathrm{COV}_{\mathrm{M}}(L,\,k_1,\,k_2;\,q)$ is the covariance of the k_1th and k_2th orders of the non-normalized moments. We then formulate $\sigma_{\mathrm{SUM}}^2(L,\,k_1,\,k_2;\,q)$ in Eq. (11). By substituting Eqs. (4) into (10),

$$\begin{aligned}\mathrm{SUM}_L(k_1,\,k_2;\,q) &= \frac{1}{L}\sum_{l=1}^{L} y_{q_{k_1},l} + \frac{1}{L}\sum_{l=1}^{L} y_{q_{k_2},l} \\ &= \frac{1}{L}\sum_{l=1}^{L}(y_{q_{k_1},l} + y_{q_{k_2},l}),\end{aligned} \tag{12}$$

which is the average of $\{y_{q_{k_1},l} + y_{q_{k_2},l}\}_{l=1,2,\cdots,L}$ following a certain model function $q_{k_1,k_2}(y)$. Similar to Eqs. (4)–(8), from the central limit theorem, $\sigma_{\mathrm{SUM}}^2(L,\,k_1,\,k_2;\,q)$ is given by

$$\begin{aligned}\sigma_{\mathrm{SUM}}^2(L,\,k_1,\,k_2;\,q) &= \frac{1}{L}\sigma_{q_{k_1,k_2}}^2 \\ &= \frac{1}{L}\mathrm{E}[(y_{q_{k_1}} + y_{q_{k_2}} - \mathrm{E}[y_{q_{k_1}} + y_{q_{k_2}}])^2] \\ &= \frac{1}{L}\mathrm{E}[(x_q^{k_1} + x_q^{k_2} - \mathrm{E}[x_q^{k_1} + x_q^{k_2}])^2] \\ &= \frac{1}{L}\{\mathrm{E}[x_q^{2k_1}] + \mathrm{E}[x_q^{2k_2}] + 2\mathrm{E}[x_q^{k_1+k_2}] - (\mathrm{E}[x_q^{k_1}] + \mathrm{E}[x_q^{k_2}])^2\} \\ &= \frac{1}{L}\{M_{\mathrm{T}}(2k_1;\,q) + M_{\mathrm{T}}(2k_2;\,q) \\ &\quad + 2M_{\mathrm{T}}(k_1 + k_2;\,q) - (M_{\mathrm{T}}(k_1;\,q) + M_{\mathrm{T}}(k_2;\,q))^2\}.\end{aligned} \tag{13}$$

Thus, by substituting Eqs. (8) and (13) into Eq. (11), the covariance $\mathrm{COV}_{\mathrm{M}}(L,\,k_1,\,k_2;q)$ is formulated as

$$\begin{aligned}\mathrm{COV}_{\mathrm{M}}(L,\,k_1,\,k_2;\,q) &= \frac{1}{2}(\sigma_{\mathrm{SUM}}^2(L,\,k_1,\,k_2;\,q) \\ &\quad - \sigma_{\mathrm{M}}^2(L,\,k_1;\,q) - \sigma_{\mathrm{M}}^2(L,\,k_2;\,q)) \\ &= \frac{1}{L}(M_{\mathrm{T}}(k_1 + k_2;\,q) - M_{\mathrm{T}}(k_1;\,q)M_{\mathrm{T}}(k_2;\,q)),\end{aligned} \tag{14}$$

which shows that the covariance of the k_1th and k_2th orders of the non-normalized moments can be determined from the number of independent samples, L, and the theoretical k_1th, k_2th, and $(k_1 + k_2)$th orders of the non-normalized moments given by Eq. (1).

2.3. Quantification of statistical variance and covariance of normalized moments

Let $\{x_{\mathrm{N},q,l}\}_{l=1,2,\cdots,L}$ be L independent random numbers normalized by the root of their power, i.e. the root of the second-order of the non-normalized moment, as follows:

$$x_{\mathrm{N},q,l} = \frac{x_{q,l}}{\sqrt{\frac{1}{L}\sum_{l=1}^{L} x_{q,l}^2}} = \frac{x_{q,l}}{\sqrt{M_L(2;\,q)}}. \tag{15}$$

The kth order of the normalized moment $M_{\mathrm{N},L}(k;q)$ obtained from $\{x_{\mathrm{N},q,l}\}_{l=1,2,\cdots,L}$ is given by:

$$\begin{aligned}M_{\mathrm{N},L}(k;\,q) &= \frac{1}{L}\sum_{l=1}^{L} x_{\mathrm{N},q,l}^k = \frac{1}{L}\sum_{l=1}^{L}\left(\frac{x_{q,l}}{\sqrt{M_L(2;\,q)}}\right)^k \\ &= \frac{M_L(k;\,q)}{M_L(2;\,q)^{\frac{k}{2}}}.\end{aligned} \tag{16}$$

Thus, the kth order of the normalized moment $M_{\mathrm{N},L}(k;q)$ is determined from the second and kth orders of the non-normalized moments; therefore, from the law of error propagation, the statistical variance $\sigma_{\mathrm{M_N}}^2(L,\,k;q)$ of $M_{\mathrm{N},L}(k;q)$ is given by

$$\begin{aligned}\sigma_{\mathrm{M_N}}^2(L,\,k;\,q) &= \left(\frac{\partial M_{\mathrm{N,T}}(k;q)}{\partial M_{\mathrm{T}}(k;q)}\right)^2 \sigma_{\mathrm{M}}^2(L,\,k;\,q) \\ &\quad + \left(\frac{\partial M_{\mathrm{N,T}}(k;q)}{\partial M_{\mathrm{T}}(2;q)}\right)^2 \sigma_{\mathrm{M}}^2(L,\,2;\,q) \\ &\quad + 2\frac{\partial M_{\mathrm{N,T}}(k;q)}{\partial M_{\mathrm{T}}(k;q)}\frac{\partial M_{\mathrm{N,T}}(k;q)}{\partial M_{\mathrm{T}}(2;q)}\mathrm{COV}_{\mathrm{M}}(L,\,k,\,2;\,q) \\ &= \frac{1}{L}\left\{\frac{M_{\mathrm{T}}(2k;q) - M_{\mathrm{T}}(k;q)^2}{M_{\mathrm{T}}(2;q)^k}\right\} \\ &\quad + \frac{1}{L}\left\{\frac{k^2 \cdot M_{\mathrm{T}}(k;q)^2}{4} \times \frac{M_{\mathrm{T}}(4;q) - M_{\mathrm{T}}(2;q)^2}{M_{\mathrm{T}}(2;q)^{k+2}}\right\} \\ &\quad - \frac{1}{L}\left\{kM_{\mathrm{T}}(k;\,q) \times \frac{M_{\mathrm{T}}(k+2;q) - M_{\mathrm{T}}(k;q)M_{\mathrm{T}}(2;q)}{M_{\mathrm{T}}(2;q)^{k+1}}\right\},\end{aligned} \tag{17}$$

where

$$M_{\mathrm{N,T}}(k;\,q) = \frac{M_{\mathrm{T}}(k;\,q)}{M_{\mathrm{T}}(2;\,q)^{\frac{k}{2}}}. \tag{18}$$

The last equation in Eq. (17) can be obtained by substituting Eqs. (8), (14), and (18) into the first equation in Eq. (17). Thus, the statistical variance of the kth order of the normalized moment, $\sigma_{\mathrm{M_N}}^2(L,\,k;\,q)$, is determined by the number of independent samples, L, and the theoretical second, fourth, kth, $(2k)$th, and $(k + 2)$th orders of the non-normalized moments given by Eq. (1).

Finally, similar to the derivation of the covariance of the non-normalized moment in Eqs. (9)–(14), the covariance

© 2023 The Japan Society of Applied Physics

$\mathrm{COV}_{\mathrm{M_N}}(L, k_1, k_2; q)$ for the normalized moment $M_{\mathrm{N},L}(k; q)$ can be derived from the law of error propagation as follows:

$$\begin{aligned}
&\mathrm{COV}_{\mathrm{M_N}}(L, k_1, k_2; q) \\
&= \frac{1}{L}\left\{\frac{M_{\mathrm{T}}(k_1+k_2;q) - M_{\mathrm{T}}(k_1;q)M_{\mathrm{T}}(k_2;q)}{M_{\mathrm{T}}(2;q)^{\frac{k_1+k_2}{2}}}\right\} \\
&+ \frac{1}{L}\left\{\frac{k_1k_2M_{\mathrm{T}}(k_1;q)M_{\mathrm{T}}(k_2;q)}{4} \times \frac{M_{\mathrm{T}}(4;q) - M_{\mathrm{T}}(2;q)^2}{M_{\mathrm{T}}(2;q)^{\frac{k_1+k_2+4}{2}}}\right\} \\
&- \frac{1}{L}\left\{\frac{k_1M_{\mathrm{T}}(k_1;q)}{2} \times \frac{M_{\mathrm{T}}(k_2+2;q) - M_{\mathrm{T}}(k_2;q)M_{\mathrm{T}}(2;q)}{M_{\mathrm{T}}(2;q)^{\frac{k_1+k_2+2}{2}}}\right\} \\
&- \frac{1}{L}\left\{\frac{k_2M_{\mathrm{T}}(k_2;q)}{2} \times \frac{M_{\mathrm{T}}(k_1+2;q) - M_{\mathrm{T}}(k_1;q)M_{\mathrm{T}}(2;q)}{M_{\mathrm{T}}(2;q)^{\frac{k_1+k_2+2}{2}}}\right\}. \qquad (19)
\end{aligned}$$

A detailed derivation of Eq. (19) is described in the appendix. Thus, the covariance $\mathrm{COV}_{\mathrm{M_N}}(L, k_1, k_2; q)$ for normalized moments is determined from the number of independent samples, L, and the theoretical second, fourth, k_1th, k_2th, $(k_1 + 2)$th, $(k_2 + 2)$th, and $(k_1 + k_2)$th orders of the non-normalized moments given by Eq. (1).

3. Methods

3.1. Mixture model of Nakagami distributions

To validate the proposed principles, we evaluated the mixture model of Nakagami distributions because this model can express several model functions used for ultrasound tissue characterization, such as Rayleigh,[3–5] Nakagami,[6–8] multi-Rayleigh,[15–18] and double-Nakagami[19–22] models. The N-component mixture model of the Nakagami distributions, $q_{\mathrm{MN}}(x|\{\alpha_i, m_i, \Omega_i\}_{i=1,2,\cdots,N})$, is defined as follows:

$$\begin{aligned}
&q_{\mathrm{MN}}(x|\{\alpha_i, m_i, \Omega_i\}_{i=1,2,\cdots,N}) \\
&= \sum_{i=1}^{N}\{\alpha_i q_{\mathrm{N}}(x|m_i, \Omega_i)\}, \left(\sum_{i=1}^{N}\alpha_i = 1\right), \qquad (20)
\end{aligned}$$

where

$$q_{\mathrm{N}}(x|m, \Omega) = \frac{2m^m x^{2m-1}}{\Gamma(m)\Omega^m}\exp\left(-\frac{mx^2}{\Omega}\right). \qquad (21)$$

Here, α_i denotes the mixture rate of a single-Nakagami distribution $q_{\mathrm{N}}(x|m_i, \Omega_i)$. m_i and Ω_i are the Nakagami parameter related to the scatterer distribution condition and the scale factor related to the power of the echo envelope amplitudes, respectively. $\Gamma(\cdot)$ denotes gamma function. $q_{\mathrm{MN}}(x|\{\alpha_i, m_i, \Omega_i\}_{\mathrm{i}=1,2,\cdots,\mathrm{N}})$ contains a single-Rayleigh ($N = 1$, $m_1 = 1$), single-Nakagami ($N = 1$), a multi-Rayleigh with N-components ($m_i = 1$ for all $i = 1, 2, \cdots, N$), and double-Nakagami ($N = 2$) models.

The theoretical kth order of the non-normalized moment for a single-Nakagami distribution $q_{\mathrm{N}}(x|m, \Omega)$ is given by[8]

$$\begin{aligned}
M_{\mathrm{T}}(k; q_{\mathrm{N}}(x|m, \Omega)) &= \int_0^\infty x^k q_{\mathrm{N}}(x|m, \Omega)dx \\
&= \frac{\Gamma\left(m+\frac{k}{2}\right)}{\Gamma(m)}\left(\frac{\Omega}{m}\right)^{\frac{k}{2}}. \qquad (22)
\end{aligned}$$

From Eqs. (1), (20), and (22), the theoretical kth order of the non-normalized moment for $q_{\mathrm{MN}}(x|\{\alpha_i, m_i, \Omega_i\}_{i=1,2,\cdots,N})$ is given by

$$\begin{aligned}
&M_{\mathrm{T}}(k; q_{\mathrm{MN}}(x|\{\alpha_i, m_i, \Omega_i\}_{i=1,2,\cdots,N})) \\
&= \int_0^\infty x^k q_{\mathrm{MN}}(x|\{\alpha_i, m_i, \Omega_i\}_{i=1,2,\cdots,N})dx \\
&= \sum_{i=1}^{N}\left\{\alpha_i \int_0^\infty x^k q_{\mathrm{N}}(x|m_i, \Omega_i)dx\right\} \\
&= \sum_{i=1}^{N}\left\{\alpha_i \frac{\Gamma\left(m_i+\frac{k}{2}\right)}{\Gamma(m_i)}\left(\frac{\Omega_i}{m_i}\right)^{\frac{k}{2}}\right\}. \qquad (23)
\end{aligned}$$

3.2. Validation of proposed principles by random number simulation

To validate the proposed principles, we evaluated the statistical variance and covariance of moments for random numbers generated using MATLAB R2020b (MathWorks Inc., Natick, Massachusetts, USA). We generated L independent random numbers $\{x_{q_{\mathrm{MN}},l}\}_{l=1,2,\cdots,L}$ following the mixture model of Nakagami distributions, $q_{\mathrm{MN}}(x|\{\alpha_i, m_i, \Omega_i\}_{i=1,2,\cdots,N})$ given by Eq. (20). Thereafter, the non-normalized moments $M_L(k; q_{\mathrm{MN}})$ and the normalized moments $M_{\mathrm{N},L}(k; q_{\mathrm{MN}})$ for these L independent random numbers were obtained using Eqs. (2) and (16), respectively. This simulation was iterated 10 000 times, and the variance and covariance for 10 000 sets of moments were compared with the theoretical statistical variance and covariance derived using the proposed principles.

3.3. Demonstration of use of proposed principles: quantification of statistical variance of Nakagami parameter estimated by moment method

The theoretical Nakagami parameter, $m = m_{\mathrm{T}}$ in Eq. (21), is related to the expectation and variance of the square of variables $\{x_{q_{\mathrm{N}}}\}$ following the Nakagami distribution.[6] This relationship can be expressed using the moments as follows:

$$\begin{aligned}
m_{\mathrm{T}} &= \frac{(\mathrm{E}[x_{q_{\mathrm{N}}}^2])^2}{\mathrm{E}[(x_{q_{\mathrm{N}}}^2 - \mathrm{E}[x_{q_{\mathrm{N}}}^2])^2]} = \frac{(\mathrm{E}[x_{q_{\mathrm{N}}}^2])^2}{\mathrm{E}[x_{q_{\mathrm{N}}}^4] - (\mathrm{E}[x_{q_{\mathrm{N}}}^2])^2} \\
&= \frac{M_{\mathrm{T}}(2; q_{\mathrm{N}})^2}{M_{\mathrm{T}}(4; q_{\mathrm{N}}) - M_{\mathrm{T}}(2; q_{\mathrm{N}})^2} = \frac{1}{\frac{M_{\mathrm{T}}(4; q_{\mathrm{N}})}{M_{\mathrm{T}}(2; q_{\mathrm{N}})^2} - 1} \\
&= \frac{1}{M_{\mathrm{N,T}}(4; q_{\mathrm{N}}) - 1}, \qquad (24)
\end{aligned}$$

where the last equation is obtained using Eq. (18). Based on Eq. (24), the moment method estimates the Nakagami parameter m as follows:

$$\hat{m} = \frac{1}{\frac{M_L(4; q_{\mathrm{N}})}{M_L(2; q_{\mathrm{N}})^2} - 1} = \frac{1}{M_{\mathrm{N},L}(4; q_{\mathrm{N}}) - 1}. \qquad (25)$$

Based on the law of error propagation, the statistical variance $\sigma_{\hat{m}}^2(L; m_{\mathrm{T}})$ of the Nakagami parameter $\hat{m}$ estimated using Eq. (25) is determined by

$$\begin{aligned}
\sigma_{\hat{m}}^2(L; m_{\mathrm{T}}) &= \left(\frac{\partial m_{\mathrm{T}}}{\partial M_{\mathrm{N,T}}(4; q_{\mathrm{N}})}\right)^2 \sigma_{\mathrm{M_N}}^2(L, 4; q_{\mathrm{N}}) \\
&= \frac{\sigma_{\mathrm{M_N}}^2(L, 4; q_{\mathrm{N}})}{(M_{\mathrm{N,T}}(4; q_{\mathrm{N}}) - 1)^4} = m_{\mathrm{T}}^4 \sigma_{\mathrm{M_N}}^2(L, 4; q_{\mathrm{N}}). \qquad (26)
\end{aligned}$$

By substituting Eq. (17) into Eq. (26), $\sigma_{\hat{m}}^2(L; m_{\mathrm{T}})$ is obtained as follows:

© 2023 The Japan Society of Applied Physics

$$\sigma^2_{\hat{m}}(L; m_T) = \frac{m_T^4}{L}\left\{\frac{M_T(8; q_N) - M_T(4; q_N)^2}{M_T(2; q_N)^4} + \frac{4M_T(4; q_N)^3}{M_T(2; q_N)^6} - \frac{4M_T(4; q_N)M_T(6; q_N)}{M_T(2; q_N)^5}\right\}, \tag{27}$$

where the theoretical moments $M_T(k; q_N)$ can be obtained using Eq. (22). Thus, the statistical variance of the Nakagami parameter $\hat{m}$ estimated by the moment method is determined by the true Nakagami parameter m_T, the number of independent samples, L, and the theoretical non-normalized moments with second, fourth, sixth, and eighth orders.

To validate Eq. (27), a random number simulation was conducted under the same conditions as those described in Sect. 3.2. The fourth order of the normalized moment $M_{N,L}(4; q_N)$ was obtained from random numbers generated from the Nakagami distribution, and the Nakagami parameter m was estimated from $M_{N,L}(4; q_N)$ using the moment method of Eq. (25).

3.4. Determination of effective number of independent samples in ultrasonic measurements

As shown by the proposed principles, the statistical variance and covariance of moments can be determined using the number of independent samples, L, and the theoretical moments $M_T(k; q)$. In ultrasonic measurements, the number of independent samples, L, is determined by the ratio of the area of analysis ROI, A_{ROI}, and the area of the ultrasound PSF, A_{PSF}, because the samples within the PSF area are correlated with each other. However, the ultrasound PSF becomes a continuous function; therefore, it is necessary to determine the effective PSF area that determines the number of independent samples, L. In this study, we define the PSF area $A_{PSF}(\geqslant\rho)$ as the area of the PSF that is equal to or larger than the threshold value $\rho(<0)$ [dB] under the condition that the amplitudes of the PSF are normalized by their maximum. Using $A_{PSF}(\geqslant\rho)$, we defined the effective number of independent samples, $L_{US}(A_{ROI}; A_{PSF}(\geqslant\rho))$, for ultrasonic measurements as follows:

$$L_{US}(A_{ROI}; A_{PSF}(\geqslant\rho)) = \frac{A_{ROI}}{A_{PSF}(\geqslant\rho)}. \tag{28}$$

Here, the ROI area A_{ROI} is defined under the condition that the width and height of the ROI are set larger than those of the PSF ($\geqslant\rho$) region. This condition is generally satisfied in a statistics-based analysis of echo envelope amplitudes. Additionally, it is assumed that the depth and lateral sampling intervals are smaller than the height and width of the ultrasound spatial resolution, respectively, and this condition is generally satisfied. Equation (28) shows the effective number of PSF ($\geqslant\rho$) that can be arranged in the ROI area without overlap. To determine the optimal $\hat{\rho}$, we conducted an ultrasonic simulation using Field II developed by Jensen et al.[36,37]

Several point scatterers were randomly and densely ($\geqslant$ 10 scatterers/$A_{PSF}(\geqslant -3$ dB)) distributed in the ultrasonic measurement region to simulate the conditions of Rayleigh distribution q_{RA}. Ultrasound RF signals scattered from the point scatterers and received by the transducer were simulated using Field II. Two types of transmitted frequencies, 3.5 and 7.5 MHz, were used to simulate the different sizes of the PSF. The sampling frequency was set to 40 MHz. The width of the element was set to the wavelength at a sound speed of 1540 m s^{-1} for each transmitted frequency. The gap between adjacent elements was set to 0.1 mm for both transmitted frequencies. Thus, the element pitch was 0.540 mm for 3.5 MHz and 0.305 mm for 7.5 MHz. The 64 elements were activated with an apodization of the Hanning window for transmitting and receiving a single beam. The impulse response of the element was set to two cycles of a sinusoidal wave with a Hanning window weight, and the excited signal was set to two cycles of a non-weighted sinusoidal wave. A transducer with 64 elements was moved in the lateral direction at intervals of the element pitch to simulate the electronic scan. In the simulation for calculating the PSF area, however, the transducer was moved at intervals of 0.010 mm to accurately calculate the PSF area with sufficiently high lateral sampling.

To determine the optimal threshold value $\hat{\rho}$ [dB], it is necessary to simulate the ultrasound echo envelope amplitudes that completely follow the Rayleigh distribution; therefore, the depth dependences of the PSF and acoustic pressure must be removed in this analysis. Thus, we used the dynamic focus technique in the depth direction, and the transmitted focused depths were dynamically changed in 1 mm intervals. All 64 elements were used for transmitting the ultrasonic beam, and all 64 element signals were used for the received beamforming, regardless of the focus depth. To compensate for the depth-dependence of the acoustic pressure, the obtained RF signals were normalized by the preliminary simulated acoustic pressure property in the depth direction.

The ROI was set for the simulated echo envelope data, and the moment was calculated for the echo envelope amplitudes in the ROI. The height of the ROI was set to 5 mm for 3.5 MHz and to 3 mm for 7.5 MHz by considering the depth dependence of the PSF. The width of the ROI was changed from 2.16 to 88.56 mm in 2.7 mm intervals for 3.5 MHz, and from 1.2 to 47.7 mm in 1.5 mm intervals for 7.5 MHz. To determine the optimal threshold value $\hat{\rho}$, a broad range of widths was examined, including the wide width condition, which is not used in the actual measurement. Subsequently, the first and third orders of non-normalized moments, $M_{US,k=1}(n; A_{ROI})$ and $M_{US,k=3}(n; A_{ROI})$, were calculated independently for each ROI area A_{ROI}. The 500 kinds ($n = 1, 2, \cdots, 500$) of echo envelope data were simulated by randomly changing the positions of the scatterers. Thereafter, the variance for 500 sets of moments, $V_{US,k}(A_{ROI})$, was calculated for each ROI area A_{ROI} as follows:

$$V_{US,k}(A_{ROI}) = \frac{1}{500}\sum_{n=1}^{500}(M_{US,k}(n; A_{ROI}) - \overline{M_{US,k}(n; A_{ROI})})^2, \tag{29}$$

where $\overline{M_{US,k}(n; A_{ROI})}$ is the average of the 500 kinds of moments $\{M_{US,k}(n; A_{ROI})\}_{n=1,2,\cdots,500}$.

The PSF area $A_{PSF}(\geqslant\rho)$ was measured for each threshold value ρ [dB]. The effective number of independent samples, $L_{US}(A_{ROI}; A_{PSF}(\geqslant\rho))$, was defined by Eq. (28). Thereafter, the theoretical variance $\sigma^2_M(L_{US}(A_{ROI}; A_{PSF}(\geqslant\rho)), k; q_{RA})$ was estimated for each ROI area A_{ROI} by substituting $L_{US}(A_{ROI}; A_{PSF}(\geqslant\rho))$ for L in Eq. (8). For each ρ, the root-

© 2023 The Japan Society of Applied Physics

mean-squared error (RMSE) of the measured variances of the moments from the theoretical variances was evaluated, and the optimal threshold value $\hat{\rho}$ was determined by minimizing the RMSE, as follows:

$$\hat{\rho} = \underset{\rho}{\operatorname{argmin}}\{RMSE_k(\rho)\}, \tag{30}$$

$$RMSE_k(\rho) = \sqrt{\mathrm{E}_{A_{\mathrm{ROI}}}[\{V_{\mathrm{US},k}(A_{\mathrm{ROI}}) - \sigma_{\mathrm{M}}^2(L_{\mathrm{US}}(A_{\mathrm{ROI}}; A_{\mathrm{PSF}}(\geqslant\rho)), k; q_{\mathrm{RA}})\}^2]}. \tag{31}$$

4. Results

4.1. Validation of principles by random number simulation

Figure 2 shows the results for the Rayleigh distribution $q_{\mathrm{RA}}(x) = q_{\mathrm{MN}}(x|\{\alpha_1 = 1, m_1 = 1, \Omega_1 = 1\}_{N=1})$. Figure 2(a) shows the probability density function of the theoretical Rayleigh distribution. Figures 2(b-i) and 2(b-ii) show the averages and standard deviations of the (b-i) first and (b-ii) third orders of the non-normalized moments M_L. The results of the random number simulations for 10 000 trials are plotted in black, using an error bar. The theoretical non-normalized moment $M_{\mathrm{T}}(k; q_{\mathrm{RA}})$ obtained using Eq. (1) is plotted as a red dashed line, and the theoretical standard deviation $\sigma_{\mathrm{M}}(L, k; q_{\mathrm{RA}})$ obtained using Eq. (8) is plotted as $M_{\mathrm{T}}(k; q_{\mathrm{RA}}) \pm \sigma_{\mathrm{M}}(L, k; q_{\mathrm{RA}})$ by red solid lines. Figures 2(c-i) and 2(c-ii) show the averages and standard deviations of the (c-i) first and (c-ii) third orders of the normalized moments $M_{\mathrm{N},L}$, plotted using the same line types and colors as in Figs. 2(b-i) and 2(b-ii). Figures 2(b-iii) and 2(c-iii) show the covariance between the first and third orders of the non-normalized moments and that of the normalized moments, respectively. The simulation results for 10 000 trials are plotted using black dots and the theoretical covariances $\mathrm{COV}_{\mathrm{M}}(L, 1, 3; q_{\mathrm{RA}})$ and $\mathrm{COV}_{\mathrm{M_N}}(L, 1, 3; q_{\mathrm{RA}})$ are plotted using solid red lines.

As shown in Fig. 2(b), the average, standard deviation, and covariance for the non-normalized moments $M_L(k; q_{\mathrm{RA}})$ corresponded well with the theoretical values $M_{\mathrm{T}}(k; q_{\mathrm{RA}})$, $\sigma_{\mathrm{M}}(L, k; q_{\mathrm{RA}})$, and $\mathrm{COV}_{\mathrm{M}}(L, k_1, k_2; q_{\mathrm{RA}})$, respectively. For the normalized moments $M_{\mathrm{N},L}(k; q_{\mathrm{RA}})$ shown in Fig. 2(c), the results for random numbers corresponded well with the theoretical values $M_{\mathrm{N,T}}(k; q_{\mathrm{RA}})$, $\sigma_{\mathrm{M_N}}(L, k; q_{\mathrm{RA}})$, and $\mathrm{COV}_{\mathrm{M_N}}(L, k_1, k_2; q_{\mathrm{RA}})$, respectively, for a large number of independent samples. However, bias errors are observed for a small number of independent samples. This may be because the number of independent samples was insufficient to satisfy the central limit theorem. By comparing Figs. 2(b) and 2(c), it was confirmed that the statistical variance could be suppressed by normalizing the moments.

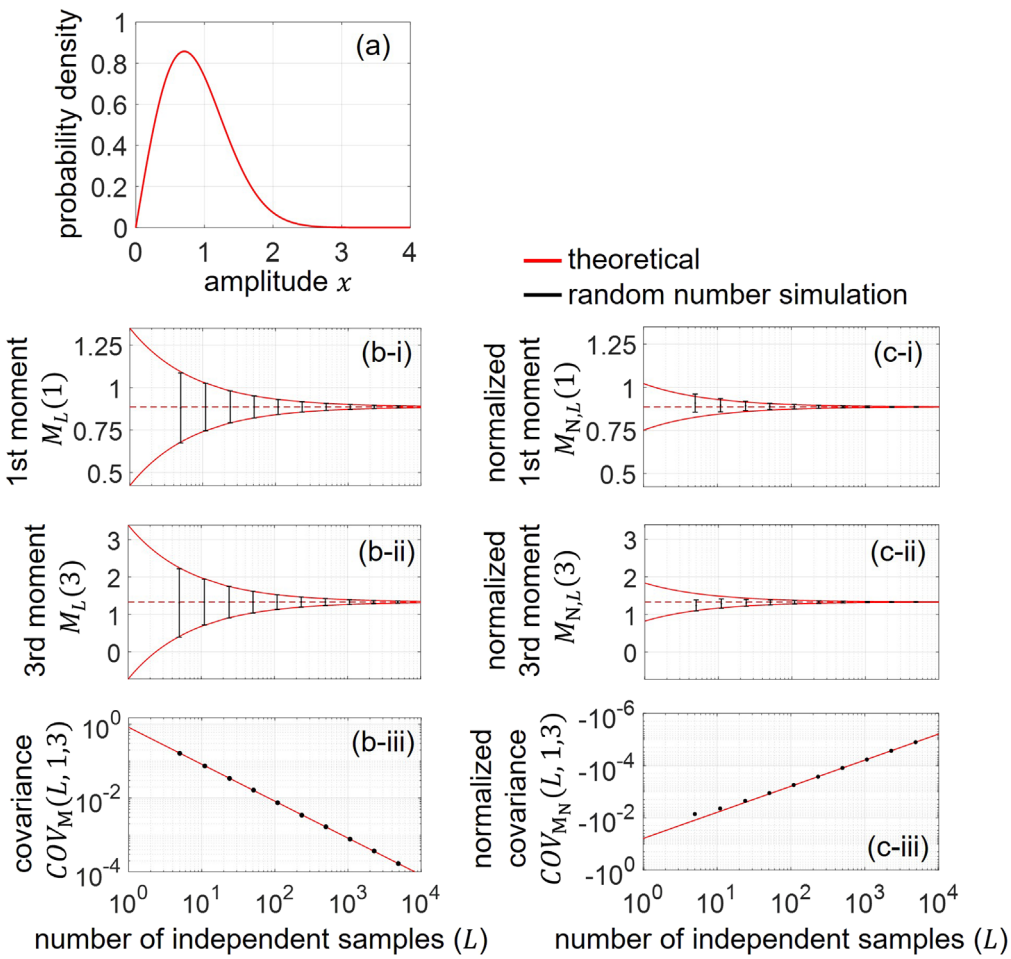

Fig. 2. (a) Probability density function of Rayleigh distribution. (i), (ii) Averages and standard deviations of (i) first and (ii) third orders of moments. (iii) Covariances of first and third orders of moments. (b) Results for non-normalized moments M_L. (c) Results for normalized moments $M_{\mathrm{N},L}$. Black: simulation results using random numbers. Red: theoretical values determined by proposed principles.

© 2023 The Japan Society of Applied Physics

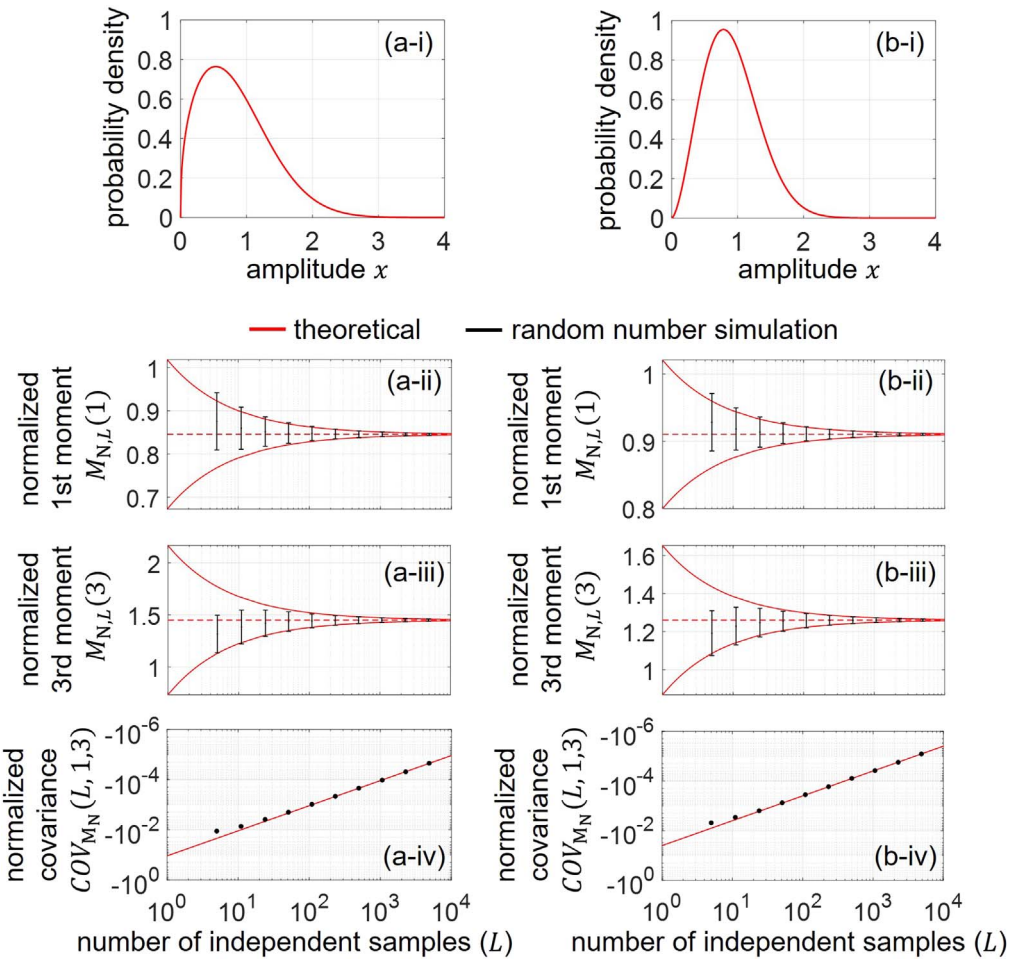

Fig. 3. (a), (b) Results for Nakagami model with model parameters (m_1, Ω_1) of (a) (0.7, 1) and (b) (1.3, 1). (i) Probability density of model function. (ii, iii) Averages and standard deviations of (ii) first and (iii) third orders of normalized moments. (iv) Covariances of first and third orders of normalized moments. Black: simulation results using random numbers. Red: theoretical values determined by proposed principles.

Similar relationships between the non-normalized and normalized moments were obtained for other model functions of the single-Nakagami, multi-Rayleigh, and double-Nakagami models. Therefore, we only show the results for the normalized moments $M_{N,L}(k;\, q)$ for these model functions. Figure 3 shows the results for the single Nakagami model [$N = 1$ in Eq. (20)]. The model parameters (m_1, Ω_1) are (0.7, 1) in Fig. 3(a) (condition pre-Rayleigh: low scattered density) and (1.3, 1) in Fig. 3(b) (condition post-Rayleigh: existence of periodically located or specular scatterers). Figures 4(a) and 4(b) show the results for the multi-Rayleigh ($\alpha_1 = 0.7$, $\alpha_2 = 0.3$, $m_1 = m_2 = 1$, $\Omega_2/\Omega_1 = 4$, $N = 2$) and double-Nakagami ($\alpha_1 = 0.7$, $\alpha_2 = 0.3$, $m_1 = 0.7$, $m_2 = 1.2$, $\Omega_2/\Omega_1 = 4$, $N = 2$) models. Figures 3(i) and 4(i) show the theoretical probability densities of the model functions. Figures 3(ii) and 4(ii) show the results for the averages and standard deviations of the first order of the normalized moment, Figs. 3(iii) and 4(iii) show the results for the third order, and Figs. 3(iv) and 4(iv) show the results for the covariance of the first and third orders of the normalized moments. The results were plotted using the same line types and colors as those in Fig. 2.

As shown in Figs. 3 and 4, the averages, standard deviations, and covariances of random numbers corresponded well with the theoretical values for a large number of independent samples, and the bias errors were caused by a small number of independent samples, which was similar to the results for the Rayleigh distribution shown in Fig. 2. Thus, the statistical variance and covariance for each model function can be correctly quantified by the proposed principles under the condition that the number of independent samples, L, is sufficiently large to satisfy the central limit theorem.

4.2. Demonstration of use of proposed principles: statistical variance of Nakagami parameter estimated by moment method

Figures 5(a)–5(c) show the results of the Nakagami parameter $\hat{m}$ estimated by the moment method in Eq. (25). Note that the exact same value was obtained for the use of the non-normalized moment $M_L(k;\, q_N)$ by the first equation and for the use of the normalized moment $M_{N,L}(k;\, q_N)$ by the last equation in Eq. (25). The average and standard deviation of the estimated results for 10 000 trials are shown in black using an error bar. Figures 5(a)–5(c) show the results for different numbers of independent samples, L, of 100, 500, and 1000, respectively. The theoretical $m_T \pm \sigma_{\hat{m}}(L;\, m_T)$ of the estimated Nakagami parameter $\hat{m}$, determined using Eq. (27), are plotted as solid red lines in Figs. 5(a)–5(c).

Although random numbers were generated from the Nakagami distribution without any noise, there were bias errors in the average of the estimated $\hat{m}$ when the number of independent samples, L, was 100, as shown in Fig. 5(a). When the number of independent samples, L, was 500 or

 © 2023 The Japan Society of Applied Physics

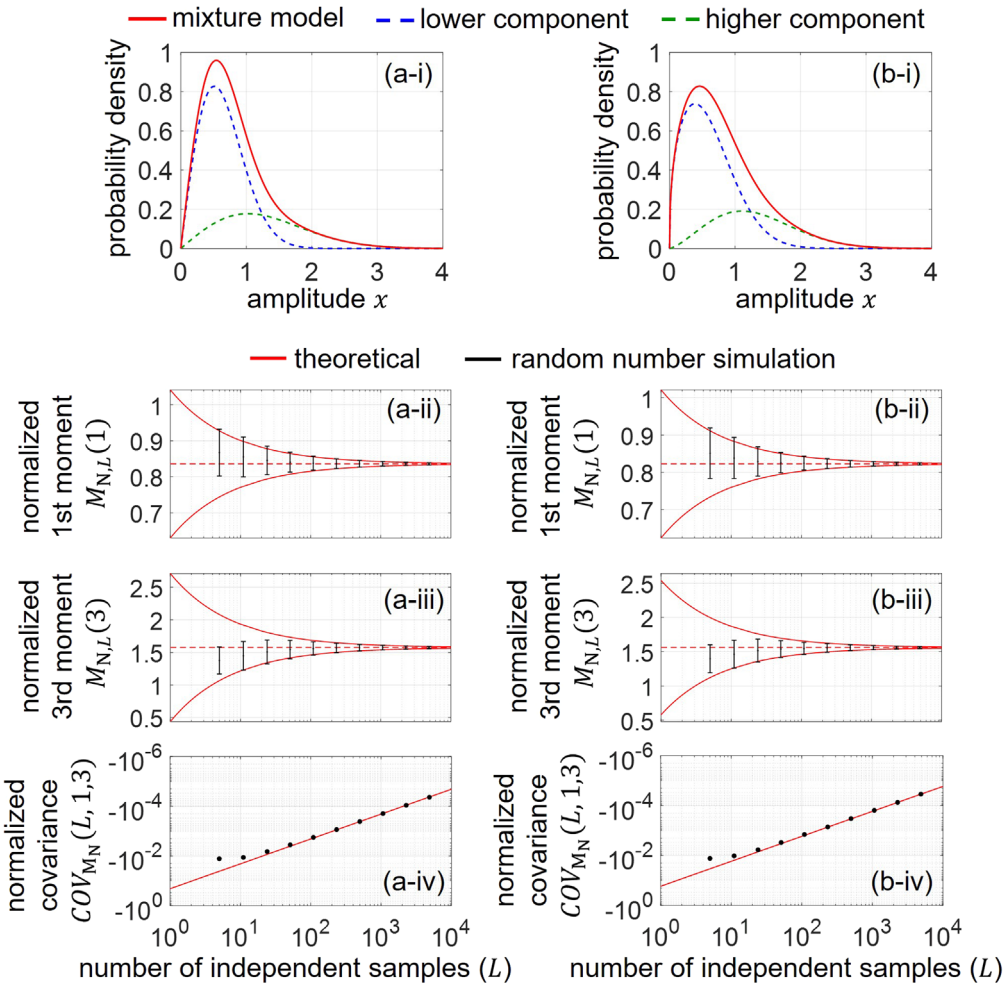

Fig. 4. (a) Results for multi-Rayleigh model with model parameters ($\alpha_1 = 0.7$, $\alpha_2 = 0.3$, $m_1 = m_2 = 1$, $\Omega_2/\Omega_1 = 4$, $N = 2$). (b) Results for double-Nakagami model with model parameters ($\alpha_1 = 0.7$, $\alpha_2 = 0.3$, $m_1 = 0.7$, $m_2 = 1.2$, $\Omega_2/\Omega_1 = 4$, $N = 2$). (i) Probability density of model function. (ii), (iii) Averages and standard deviations of (ii) first and (iii) third orders of normalized moments. (iv) Covariances of first and third orders of normalized moments. Black: simulation results using random numbers. Red: theoretical values determined by proposed principles.

1000, the standard deviation of the estimated $\hat{m}$ corresponded well with the theoretical standard deviation $\sigma_{\hat{m}}(L; m_T)$ obtained from Eq. (27). Thus, it was confirmed that the proposed principle can correctly quantify the standard deviation $\sigma_{\hat{m}}(L; m_T)$ of the Nakagami parameter $\hat{m}$ estimated by the moment method when the number of independent samples, L, is sufficiently large to satisfy the central limit theorem, as in the moment evaluation in Sect. 4.1.

Figure 5(d) shows the relationship between the number of independent samples, L, and the theoretical standard deviation $\sigma_{\hat{m}}(L; m_T)$ of the estimated Nakagami parameter $\hat{m}$, for each true parameter m_T. As shown in Fig. 5(d), the standard deviation becomes larger for a large Nakagami parameter m.

4.3. Determination of effective number of independent samples in an ultrasonic measurement

Figures 6(a) and 6(b) show the simulated B-mode images of PSFs for transmitted frequencies of 3.5 and 7.5 MHz, respectively. Figure 6(c) shows the relationship between the threshold value ρ [dB] and the PSF area $A_{PSF}(\geqslant\rho)$ [mm^2]. Figures 7(a) and 7(b) show examples of simulated B-mode images following the Rayleigh distribution for transmitted frequencies of 3.5 and 7.5 MHz, respectively, for an ROI width of 20 mm.

Figures 8(a) and 8(b) show the relationships between the ROI area A_{ROI} [mm^2] and the obtained variances $V_k(A_{ROI})$ of the first- and third-order non-normalized moments, respectively. As shown in Fig. 8, the variance of the moments decreased with the broadening of the ROI area A_{ROI} [mm^2]. Furthermore, for the same ROI area A_{ROI} [mm^2], the variance of the moments decreased when using a higher transmitted frequency. This is because the PSF area $A_{PSF}(\geqslant\rho)$ [mm^2] is smaller for higher transmitted frequencies, as shown in Fig. 6. Thus, the statistical variance of the moments depends on both the ROI area A_{ROI} [mm^2] and PSF area $A_{PSF}(\geqslant\rho)$ [mm^2].

Figure 9 shows the relationship between the threshold value ρ [dB] for determining the PSF area $A_{PSF}(\geqslant\rho)$ and $\mathrm{RMSE}_k(\rho)$ evaluated using Eq. (31). Because a small number of independent samples caused a bias error for normalized moments, as confirmed by Fig. 2(c), the effective number of independent samples, L_{US}, was determined from the non-normalized moments $M_L(k; q)$. Figures 9(a) and 9(b) show the results for the first- and third-order non-normalized moments, respectively. As shown in Fig. 9, $\mathrm{RMSE}_k(\rho)$ was minimized at approximately $\rho = -6$ dB. Thus, we determined the effective number of independent samples for an ROI area of A_{ROI} by $L_{US}(A_{ROI}; A_{PSF}(\geqslant\hat{\rho} = -6\ \mathrm{dB}))$.

© 2023 The Japan Society of Applied Physics

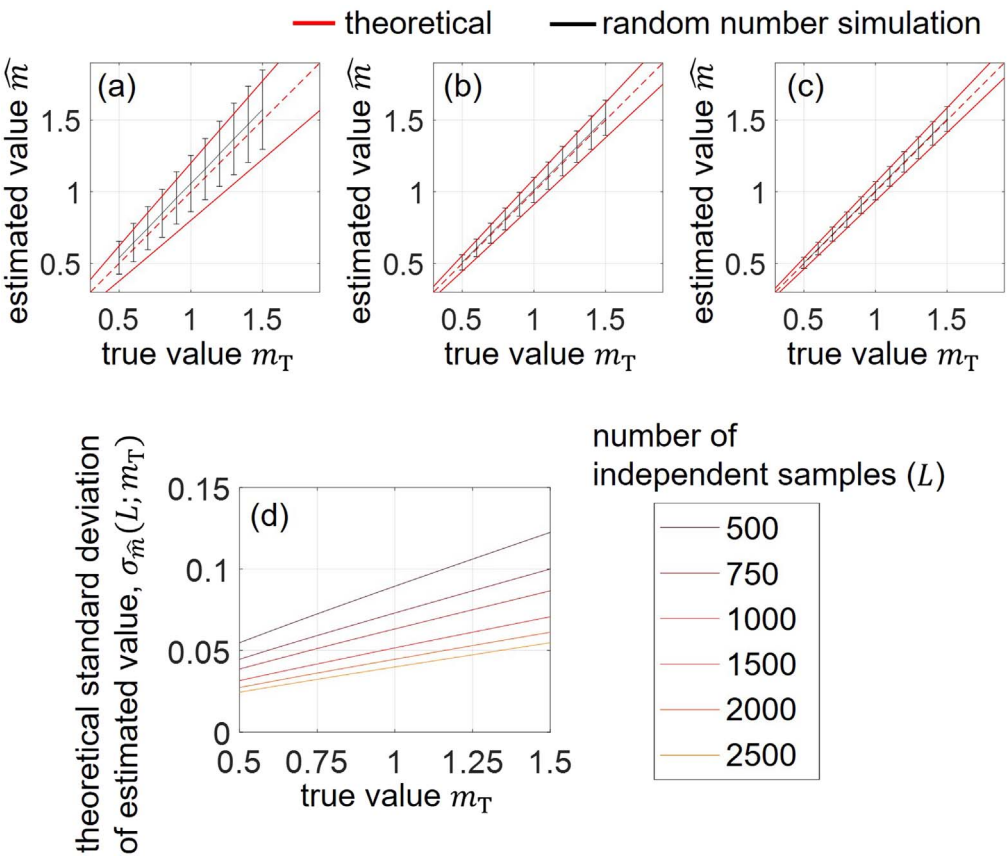

Fig. 5. Results of standard deviation of Nakagami parameter $\hat{m}$ estimated by moment method. (a), (b), (c) Relationships between Nakagami parameters $\hat{m}$ estimated from random numbers (black) and theoretically determined values (red). Number of independent samples, L, was set to (a) 100, (b) 500, and (c) 1000. (d) Relationships between true m_T and theoretical standard deviation of estimated $\hat{m}$ by moment method. Results for each number of independent samples, L, are plotted in different colors.

Figure 10 shows examples of an RMSE_k evaluation using Eqs. (30) and (31) for (a) $\rho = -10$ dB, (b) $\rho = -6$ dB, and (c) $\rho = -2$ dB. Figures 10(i) and 10(ii) show the shape of the PSF ($\geqslant\rho$) when the transmitted frequencies were 3.5 and 7.5 MHz, respectively. Figures 10(iii) and 10(iv) show the relationship between the variance of the ultrasonically simulated moments, $V_{\mathrm{US},k}(A_{\mathrm{ROI}})$, and the estimated variance $\sigma^2_{\mathrm{M}}(L_{\mathrm{US}}(A_{\mathrm{ROI}}; A_{\mathrm{PSF}}(\geqslant\rho)), k; q_{\mathrm{RA}})$ obtained using Eq. (8) under the condition that the number of independent samples, L, is $L_{\mathrm{US}}(A_{\mathrm{ROI}}; A_{\mathrm{PSF}}(\geqslant\rho))$.

When the threshold value ρ is lower than the optimal $\hat{\rho} = -6$dB, as shown in Fig. 10(a), the PSF area $A_{\mathrm{PSF}}(\geqslant -10\mathrm{dB})$ becomes large, as shown by comparing Figs. 10(a-i) and 10(b-i) or Figs. 10(a-ii) and 10(b-ii); therefore, the effective number of PSF in the ROI becomes relatively small. In this case, the determined effective number of independent samples, $L_{\mathrm{US}}(A_{\mathrm{ROI}}; A_{\mathrm{PSF}}(\geqslant -10\mathrm{dB}))$, becomes smaller than the actual number of independent samples in the ROI, and the estimated variance $\sigma^2_{\mathrm{M}}(L_{\mathrm{US}}(A_{\mathrm{ROI}}; A_{\mathrm{PSF}}(\geqslant -10\ \mathrm{dB})), k; q_{\mathrm{RA}})$ using Eq. (8) was overestimated, as shown in Figs. 10(a-iii) and 10(a-iv).

By contrast, when the threshold value ρ is higher than the optimal $\hat{\rho} = -6$ dB, as shown in Fig. 10(c), the PSF area $A_{\mathrm{PSF}}(\geqslant -2\ \mathrm{dB})$ becomes small, and the effective number of PSF in the ROI becomes relatively large. In this case, $L_{\mathrm{US}}(A_{\mathrm{ROI}}; A_{\mathrm{PSF}}(\geqslant -2\ \mathrm{dB}))$ becomes larger than the actual number of independent samples in the ROI, and the estimated variance $\sigma^2_{\mathrm{M}}(L_{\mathrm{US}}(A_{\mathrm{ROI}}; A_{\mathrm{PSF}}(\geqslant -2\ \mathrm{dB})), k; q_{\mathrm{RA}})$ using Eq. (8) was underestimated, as shown in Figs. 10(c-iii) and 10(c-iv).

Thus, in both cases shown in Figs. 10(a) and 10(c), RMSE_k in Eq. (31), which shows the deviation of the variance of the ultrasonically simulated moments, $V_{\mathrm{US},k}(A_{\mathrm{ROI}})$ (dots in Figs. 10(iii) and 10(iv)), from the theoretical variance $\sigma^2_{\mathrm{M}}(L_{\mathrm{US}}(A_{\mathrm{ROI}}; A_{\mathrm{PSF}}(\geqslant\rho)), k; q_{\mathrm{RA}})$ (red lines in Figs. 10(iii) and 10(iv)), becomes larger than that for the optimal threshold value $\hat{\rho} = -6$ dB (Fig. 10(b)), as shown in Fig. 9.

Using the optimized threshold value $\hat{\rho} = -6$ dB, the variance of the ultrasonically simulated moments, $V_{\mathrm{US},k}(A_{\mathrm{ROI}})$, corresponded well with the theoretical variance $\sigma^2_{\mathrm{M}}(L_{\mathrm{US}}(A_{\mathrm{ROI}}; A_{\mathrm{PSF}}(\geqslant\hat{\rho} = -6\ \mathrm{dB})), k; q_{\mathrm{RA}})$, as shown in Figs. 10(b-iii) and 10(b-iv). Thus, the number of independent samples, L, in the ROI area A_{ROI} can be quantified by $L_{\mathrm{US}}(A_{\mathrm{ROI}}; A_{\mathrm{PSF}}(\geqslant -6\ \mathrm{dB}))$ obtained using Eq. (28).

5. Discussion

In this study, we quantified the statistical variance and covariance of moments caused by a finite number of independent samples, L. The statistical variance and covariance can be theoretically determined from the number of independent samples, L, and the theoretical moments given by Eq. (1). Furthermore, we evaluated the relationship between the ultrasonic measurement conditions and the effective number of independent samples via ultrasonic simulation. As a result, the number of independent samples

 © 2023 The Japan Society of Applied Physics

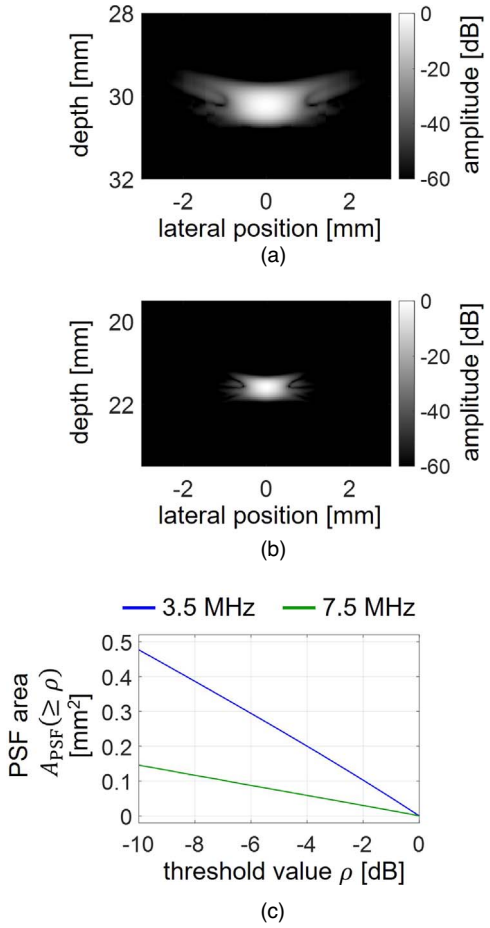

Fig. 6. (a), (b) Simulated ultrasound B-mode images of point spread function (PSF) for transmitted frequencies of (a) 3.5 and (b) 7.5 MHz. (c) Relationship between threshold value ρ [dB] and PSF area $A_{PSF}(\geqslant\rho)$ [mm^2]. Transmitted frequencies: (blue) 3.5 and (red) 7.5 MHz.

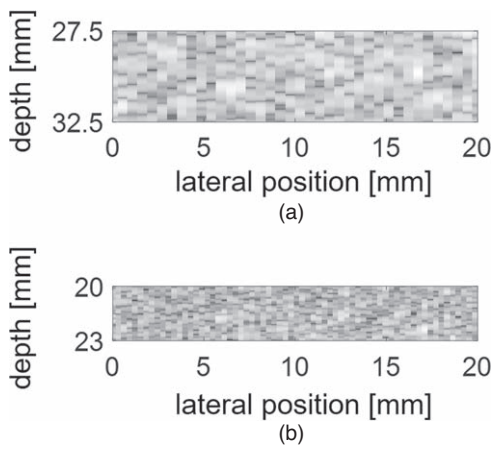

Fig. 7. Examples of simulated ultrasound B-mode images following Rayleigh distribution. Transmitted frequencies: (a) 3.5 and (b) 7.5 MHz.

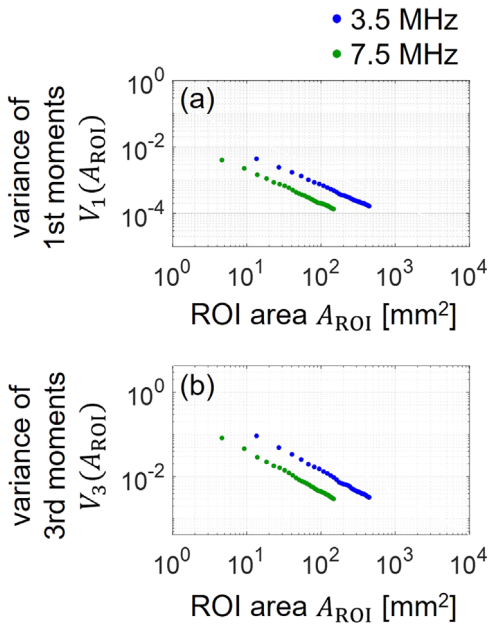

Fig. 8. Relationship between ROI area A_{ROI} [mm^2] and variance of non-normalized moments with (a) first and (b) third orders. Variance for 500 sets of non-normalized moments is plotted. Transmitted frequencies: (blue) 3.5 and (green) 7.5 MHz.

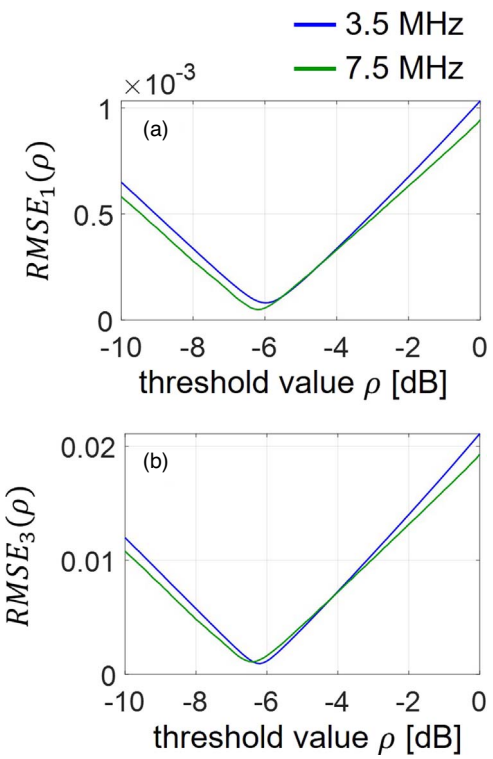

Fig. 9. Relationship between threshold value ρ [dB] for determining PSF area $A_{PSF}(\geqslant\rho)$ and root-mean-squared error $RMSE_k(\rho)$ evaluated for (a) first and (b) third orders of non-normalized moments by Eq. (31). Transmitted frequencies: (blue) 3.5 and (green) 7.5 MHz.

could be estimated by the ratio of the ROI area to the PSF ($\geqslant -6$ dB) area, $L_{US}(A_{ROI}; A_{PSF}(\geqslant -6\text{ dB}))$ given by Eq. (28).

Based on these results, we can determine the statistical limitation of the moment analysis for given ROI and PSF sizes and the model function used. Therefore, when the resolution of the moment analysis required for the target tissue characterization is determined, we can theoretically determine the necessary conditions for the ROI area and ultrasound spatial resolution (PSF area).

In the simulation results using random numbers, bias errors were present for normalized moments when the number of independent samples was insufficient, although the statistical

 © 2023 The Japan Society of Applied Physics

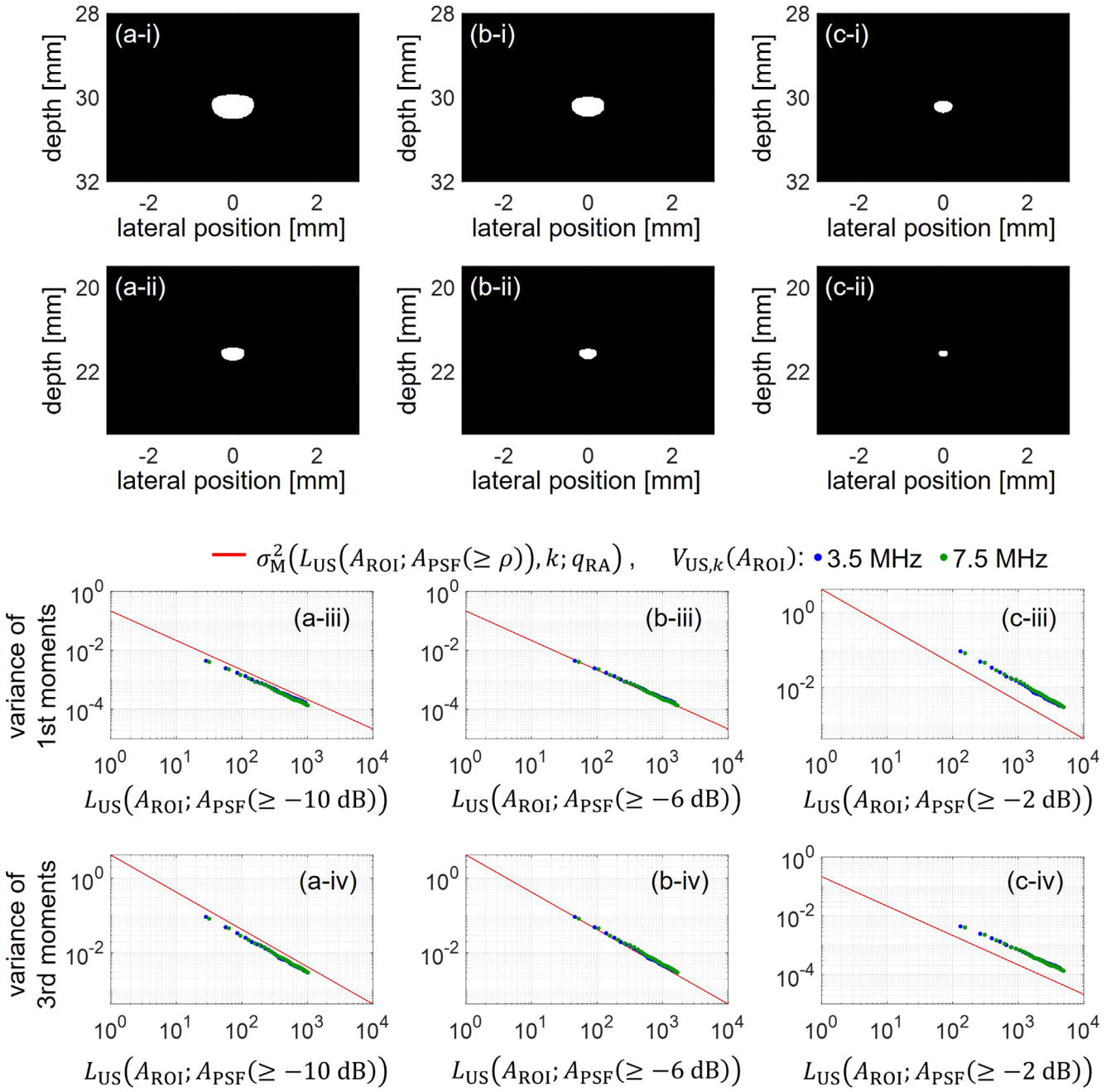

Fig. 10. (i), (ii) Shapes of PSFs that are equal to or larger than ρ [dB]. Transmitted frequencies were (i) 3.5 and (ii) 7.5 MHz. Threshold value ρ was set to (a) -10, (b) -6, and (c) -2dB. (iii), (iv) Relationships between theoretical variances and ultrasonically simulated variances of (iii) first and (iv) third orders of non-normalized moments, when $L_{US}(A_{ROI}; A_{PSF}(\geqslant \rho))$ is regarded as the number of independent samples, L. Theoretical variances of non-normalized moments are plotted using red lines, and ultrasonically simulated variances are plotted using dots. Transmitted frequencies: (blue) 3.5 and (green) 7.5 MHz.

variance could be suppressed compared with the non-normalized moments. These bias errors cause a false evaluation of the tissue characteristics; therefore, the ROI size must be carefully determined, especially when a small ROI is used to improve the locality of tissue characterization.

As shown in Fig. 5, we demonstrated the use of the proposed principles in the analysis of the statistical limitations of tissue characterization. In this study, we theoretically quantified the statistical variance of the Nakagami parameter m estimated using the moment method. The Nakagami parameter m reflects several scatterer-distribution conditions, such as the scattered density or the existence of periodically located or specular scatterers. As several scatterer-distribution conditions can be quantified using a single parameter, the Nakagami parameter has been widely used for quantitative tissue characterization, such as the quantification of liver steatosis,[7] quantification of lymph nodes,[27] and monitoring of temperature changes in biological tissues.[29–31]

As shown in Fig. 5(a), there were bias errors for the average of the estimated $\hat{m}$ by the moment method when the number of independent samples was 100. By considering the effective number of independent samples, L_{US}, in the ROI, determined by the method proposed in Sect. 3.4, it is considered that the Nakagami parameter is statistically overestimated by the moment method when the ROI area A_{ROI} is

 © 2023 The Japan Society of Applied Physics

only 100 times the PSF area $A_{\mathrm{PSF}}(\geqslant -6\ \mathrm{dB})$; $A_{\mathrm{ROI}} = 100 \times A_{\mathrm{PSF}}(\geqslant -6\ \mathrm{dB})$. Thus, the ROI size should be carefully determined to prevent overestimation of the Nakagami parameter m.

Even when the ROI area is sufficiently large and/or the PSF area is sufficiently small to avoid an overestimation of the Nakagami parameter, the statistical variance of the estimated Nakagami parameter $\hat{m}$ depends on the number of independent samples, L, i.e. the ratio of the ROI area to the PSF area, $A_{\mathrm{ROI}}/A_{\mathrm{PSF}}(\geqslant -6\ \mathrm{dB})$, as shown in Fig. 5(d). When the resolution of the Nakagami parameter estimation required for target tissue characterization is determined, the necessary conditions for the ROI and PSF areas can be quantitatively determined by the principles proposed in this paper, which is part of a future study.

In this study, we focused on the Nakagami parameter to demonstrate the use of the proposed principles. In future studies, we will quantify the statistical limitations of parameter estimations for other model functions, such as the multi-Rayleigh, double-Nakagami, and homodyned-K distributions, and develop stable tissue characterization methods.

6. Conclusions

In this study, we quantified the statistical limitations of moment analysis caused by a finite number of samples. The statistical variance and covariance can be determined from the number of independent samples and theoretical moments of the model function. Using an ultrasonic simulation, it was confirmed that the effective number of independent samples of the ultrasonic measurement could be estimated from the relationship between the areas of the ROI and PSF. The proposed principles will contribute to the quantification of the statistical limitations of statistics-based tissue characterization and the development of stable tissue characterization methods.

Acknowledgments

This work was partially supported by the Japan Society for the Promotion of Science KAKENHI (Grant No. 21K14166).

Appendix

We derive the covariance for the normalized moment in Eq. (19). Similar to Eqs. (9) and (10), we define the summation of the k_1th and k_2th orders of the normalized moments as follows:

$$\begin{aligned}\mathrm{SUM}_{\mathrm{N,T}}(k_1, k_2; q) &= M_{\mathrm{N,T}}(k_1; q) + M_{\mathrm{N,T}}(k_2; q)\\ &= \frac{M_{\mathrm{T}}(k_1; q)}{M_{\mathrm{T}}(2; q)^{\frac{k_1}{2}}} + \frac{M_{\mathrm{T}}(k_2; q)}{M_{\mathrm{T}}(2; q)^{\frac{k_2}{2}}},\end{aligned} \tag{A·1}$$

$$\begin{aligned}\mathrm{SUM}_{\mathrm{N},L}(k_1, k_2; q) &= M_{\mathrm{N},L}(k_1; q) + M_{\mathrm{N},L}(k_2; q)\\ &= \frac{M_L(k_1; q)}{M_L(2; q)^{\frac{k_1}{2}}} + \frac{M_L(k_2; q)}{M_L(2; q)^{\frac{k_2}{2}}}.\end{aligned} \tag{A·2}$$

Similar to Eqs. (11) and (14), the covariance of the normalized moment is derived based on the law of error propagation as follows:

$$\begin{aligned}\mathrm{COV}_{\mathrm{M_N}}(L, k_1, k_2; q) = \tfrac{1}{2}(&\sigma^2_{\mathrm{SUM_N}}(L, k_1, k_2; q)\\ &-\sigma^2_{\mathrm{M_N}}(L, k_1; q) - \sigma^2_{\mathrm{M_N}}(L, k_2; q)),\end{aligned} \tag{A·3}$$

where $\sigma^2_{\mathrm{SUM_N}}(L, k_1, k_2; q)$ is the statistical variance of $\mathrm{SUM}_{\mathrm{N},L}(k_1, k_2; q)$. Here, $\sigma^2_{\mathrm{M_N}}(L, k_1; q)$ and $\sigma^2_{\mathrm{M_N}}(L, k_2; q)$ are obtained using Eq. (17). Therefore, we derive $\sigma^2_{\mathrm{SUM_N}}(L, k_1, k_2; q)$, as follows:

As shown by Eq. (A·2), $\mathrm{SUM}_{\mathrm{N},L}(k_1, k_2; q)$ is composed of three different orders of moments, $M_L(k_1; q)$, $M_L(k_2; q)$, and $M_L(2; q)$. Therefore, from the law of error propagation, the statistical variance $\sigma^2_{\mathrm{SUM_N}}(L, k_1, k_2; q)$ of $\mathrm{SUM}_{\mathrm{N},L}(k_1, k_2; q)$ is derived as follows:

$$\begin{aligned}&\sigma^2_{\mathrm{SUM_N}}(L, k_1, k_2; q)\\ &= \left(\frac{\partial \mathrm{SUM}_{\mathrm{N,T}}(k_1, k_2; q)}{\partial M_{\mathrm{T}}(k_1; q)}\right)^2 \sigma^2_{\mathrm{M}}(L, k_1; q)\\ &+ \left(\frac{\partial \mathrm{SUM}_{\mathrm{N,T}}(k_1, k_2; q)}{\partial M_{\mathrm{T}}(k_2; q)}\right)^2 \sigma^2_{\mathrm{M}}(L, k_2; q)\\ &+ \left(\frac{\partial \mathrm{SUM}_{\mathrm{N,T}}(k_1, k_2; q)}{\partial M_{\mathrm{T}}(2; q)}\right)^2 \sigma^2_{\mathrm{M}}(L, 2; q)\\ &+ 2\frac{\partial \mathrm{SUM}_{\mathrm{N,T}}(k_1, k_2; q)}{\partial M_{\mathrm{T}}(k_1; q)}\frac{\partial \mathrm{SUM}_{\mathrm{N,T}}(k_1, k_2; q)}{\partial M_{\mathrm{T}}(k_2; q)}\mathrm{COV}_{\mathrm{M}}(L, k_1, k_2; q)\\ &+ 2\frac{\partial \mathrm{SUM}_{\mathrm{N,T}}(k_1, k_2; q)}{\partial M_{\mathrm{T}}(k_1; q)}\frac{\partial \mathrm{SUM}_{\mathrm{N,T}}(k_1, k_2; q)}{\partial M_{\mathrm{T}}(2; q)}\mathrm{COV}_{\mathrm{M}}(L, k_1, 2; q)\\ &+ 2\frac{\partial \mathrm{SUM}_{\mathrm{N,T}}(k_1, k_2; q)}{\partial M_{\mathrm{T}}(k_2; q)}\frac{\partial \mathrm{SUM}_{\mathrm{N,T}}(k_1, k_2; q)}{\partial M_{\mathrm{T}}(2; q)}\mathrm{COV}_{\mathrm{M}}(L, k_2, 2; q).\end{aligned} \tag{A·4}$$

Here, $\sigma^2_{\mathrm{M}}(L, k_1; q)$, $\sigma^2_{\mathrm{M}}(L, k_2; q)$, and $\sigma^2_{\mathrm{M}}(L, 2; q)$ are the statistical variances of the non-normalized moments determined using Eq. (8), and $\mathrm{COV}_{\mathrm{M}}(L, k_1, k_2; q)$, $\mathrm{COV}_{\mathrm{M}}(L, k_1, 2; q)$, and $\mathrm{COV}_{\mathrm{M}}(L, k_2, 2; q)$ are the covariances of the non-normalized moments determined using Eq. (14). Thus, $\sigma^2_{\mathrm{SUM_N}}(L, k_1, k_2; q)$ can be obtained by substituting Eqs. (8), (14), and (A·1) into Eq. (A·4). Finally, by substituting Eqs. (17) and (A·4) into Eq. (A·3), the covariance of the normalized moments, $\mathrm{COV}_{\mathrm{M_N}}(L, k_1, k_2; q)$, is determined, as shown in Eq. (19).

1) M. L. Oelze and J. Mamou, IEEE Trans. Ultrason. Ferroelectr. Freq. Control **63**, 336 (2016).
2) T. Yamaguchi, J. Med. Ultrason. **48**, 391 (2021).
3) L. Rayleigh, Philos. Mag. **10**, 73 (1880).
4) C. B. Burckhardt, IEEE Trans. Sonics Ultrason. **25**, 1 (1978).
5) R. F. Wagner, S. W. Smith, J. M. Sandrik, and H. Lopez, IEEE Trans. Sonics Ultrason. **30**, 156 (1983).
6) P. M. Shankar, IEEE Trans. Ultrason. Ferroelectr. Freq. Control **47**, 727 (2000).
7) P.-H. Tsui, M.-C. Ho, D.-I. Tai, Y.-H. Lin, C.-Y. Wang, and H.-Y. Ma, Sci. Rep. **6**, 33075 (2016).
8) P. M. Shankar, IEEE Trans. Ultrason. Ferroelectr. Freq. Control **48**, 1716 (2001).
9) V. M. Narayanan, P. M. Shankar, and J. M. Reid, IEEE Trans. Ultrason. Ferroelectr. Freq. Control **41**, 845 (1994).
10) P. M. Shankar, V. A. Dumane, J. M. Reid, V. Genis, F. Forsberg, C. W. Piccoli, and B. B. Goldberg, Ultrasound Med. Biol. **26**, 1503 (2000).
11) V. Dutt and J. F. Greenleaf, Ultrason. Imaging **16**, 265 (1994).
12) M. Omura, K. Yoshida, S. Akita, and T. Yamaguchi, Jpn. J. Appl. Phys. **57**, 07LF15 (2018).
13) F. Destrempes, E. Franceschini, F. T. H. Yu, and G. Cloutier, IEEE Trans. Med. Imaging **35**, 488 (2016).
14) Z. Zhou, Q. Zhang, W. Wu, Y.-H. Lin, D.-I. Tai, J.-H. Tseng, Y.-R. Lin, S. Wu, and P.-H. Tsui, Quant. Imaging Med. Surg. **9**, 1932 (2019).
15) Y. Igarashi, H. Ezuka, T. Yamaguchi, and H. Hachiya, Jpn. J. Appl. Phys. **49**, 07HF06 (2010).
16) S. Mori, S. Hirata, and H. Hachiya, Jpn. J. Appl. Phys. **53**, 07KF23 (2014).
17) S. Mori, S. Hirata, T. Yamaguchi, and H. Hachiya, Jpn. J. Appl. Phys. **54**, 07HF20 (2015).

 © 2023 The Japan Society of Applied Physics

18) S. Mori, S. Hirata, T. Yamaguchi, and H. Hachiya, Jpn. J. Appl. Phys. **57**, 07LF17 (2018).
19) K. Tamura, K. Yoshida, H. Maruyama, H. Hachiya, and T. Yamaguchi, Jpn. J. Appl. Phys. **57**, 07LD19 (2018).
20) K. Tamura, J. Mamou, K. Yoshida, H. Hachiya, and T. Yamaguchi, Jpn. J. Appl. Phys. **59**, SKKE23 (2020).
21) Y. Sato, K. Tamura, S. Mori, D.-I. Tai, P.-H. Tsui, K. Yoshida, S. Hirata, H. Maruyama, and T. Yamaguchi, Jpn. J. Appl. Phys. **60**, SDDE06 (2021).
22) F. Fang, J. Fang, Q. Li, D.-I. Tai, Y.-L. Wan, K. Tamura, T. Yamaguchi, and P.-H. Tsui, Diagnostics **10**, 557 (2020).
23) Z. Zhou, A. Gao, Q. Zhang, W. Wu, S. Wu, and P.-H. Tsui, Ultrason. Imaging **42**, 92 (2020).
24) T. Yamaguchi and H. Hachiya, Jpn. J. Appl. Phys. **37**, 3093 (1998).
25) B. I. Raju and M. A. Srinivasan, IEEE Trans. Ultrason. Ferroelectr. Freq. Control **49**, 871 (2002).
26) M. Omura, K. Yoshida, M. Kohta, T. Kubo, T. Ishiguro, K. Kobayashi, N. Hozumi, and T. Yamaguchi, Jpn. J. Appl. Phys. **55**, 07KF14 (2016).
27) J. Mamou, A. Coron, M. L. Oelze, E. Saegusa-Beecroft, M. Hata, P. Lee, J. Machi, E. Yanagihara, P. Laugier, and E. J. Feleppa, Ultrasound Med. Biol. **37**, 345 (2011).
28) T. M. Bui, A. Coron, J. Mamou, E. Saegusa-Beecroft, T. Yamaguchi, E. Yanagihara, J. Machi, S. L. Bridal, and E. J. Feleppa, Jpn. J. Appl. Phys. **53**, 07KF22 (2014).
29) P.-H. Tsui, Y.-C. Shu, W.-S. Chen, H.-L. Liu, I.-T. Hsiao, and Y.-T. Chien, Med. Phys. **39**, 2369 (2012).
30) M. Takeuchi, Y. Matsui, T. Sakai, G. Andocs, R. Nagaoka, and H. Hasegawa, Jpn. J. Appl. Phys. **58**, SGGE09 (2019).
31) M. Takeuchi et al., Ultrasound Med. Biol. **47**, 3301 (2021).
32) S. Mori, M. Ohashi, S. Hirata, and H. Hachiya, Jpn. J. Appl. Phys. **55**, 07KF09 (2016).
33) C. Zhang, S. Mori, S. Hirata, and H. Hachiya, Jpn. J. Appl. Phys. **57**, 07LF27 (2018).
34) C. Zhang, S. Hirata, and H. Hachiya, Jpn. J. Appl. Phys. **59**, SKKE27 (2020).
35) S. Mori, M. Arakawa, H. Kanai, and H. Hachiya, Proc. Symp. Ultrason. Electron. **43**, 323 (2022).
36) J. A. Jensen, Field: A Program for Simulating Ultrasound Systems **34**, [Suppl. 1, Part 1] 351 (1996), https://field-ii.dk/documents/jaj_nbc_1996.pdf.
37) J. A. Jensen and N. B. Svendsen, IEEE Trans. Ultrason. Ferroelectr. Freq. Control **39**, 262 (1992).

 © 2023 The Japan Society of Applied Physics